JACS
JOURNAL OF THE AMERICAN CHEMICAL SOCIETY
Article
pubs.acs.org/JACS

Tuning the Excitonic and Plasmonic Properties of Copper Chalcogenide Nanocrystals

Ilka Kriegel,[†,⊥] Chengyang Jiang,[‡,⊥] Jessica Rodríguez-Fernández,[†] Richard D. Schaller,[§,∥] Dmitri V. Talapin,*[,‡,§] Enrico da Como,*[,†] and Jochen Feldmann[†]

[†]Photonics and Optoelectronics Group, Department of Physics and CeNS, Ludwig-Maximilians-Universität München, Munich, Germany

[‡]Department of Chemistry, University of Chicago, Chicago, Illinois 60637, United States

[§]Argonne National Laboratory, Center for Nanoscale Materials, Argonne, Illinois 60439, United States

[∥]Department of Chemistry, Northwestern University, Evanston, Illinois 60208, United States

Supporting Information

ABSTRACT: The optical properties of stoichiometric copper chalcogenide nanocrystals (NCs) are characterized by strong interband transitions in the blue part of the spectral range and a weaker absorption onset up to ∼1000 nm, with negligible absorption in the near-infrared (NIR). Oxygen exposure leads to a gradual transformation of stoichiometric copper chalcogenide NCs (namely, $Cu_{2-x}S$ and $Cu_{2-x}Se$, $x = 0$) into their nonstoichiometric counterparts ($Cu_{2-x}S$ and $Cu_{2-x}Se$, $x > 0$), entailing the appearance and evolution of an intense localized surface plasmon (LSP) band in the NIR. We also show that well-defined copper telluride NCs ($Cu_{2-x}Te$, $x > 0$) display a NIR LSP, in analogy to nonstoichiometric copper sulfide and selenide NCs. The LSP band in copper chalcogenide NCs can be tuned by actively controlling their degree of copper deficiency via oxidation and reduction experiments. We show that this controlled LSP tuning affects the excitonic transitions in the NCs, resulting in photoluminescence (PL) quenching upon oxidation and PL recovery upon subsequent reduction. Time-resolved PL spectroscopy reveals a decrease in exciton lifetime correlated to the PL quenching upon LSP evolution. Finally, we report on the dynamics of LSPs in nonstoichiometric copper chalcogenide NCs. Through pump−probe experiments, we determined the time constants for carrier-phonon scattering involved in LSP cooling. Our results demonstrate that copper chalcogenide NCs offer the unique property of holding excitons and highly tunable LSPs on demand, and hence they are envisaged as a unique platform for the evaluation of exciton/LSP interactions.

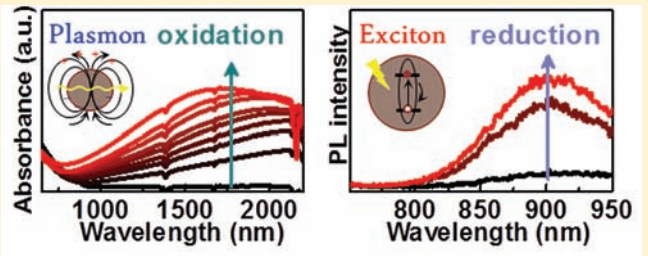

1. INTRODUCTION

Transition-metal chalcogenide nanocrystals (NCs) based on earth-abundant transition metals like copper have generated a great deal of attention as building blocks for low-cost, solution-processed, photovoltaic applications.[1,2] Cu_2S and its derived copper-deficient structures ($Cu_{2-x}S$, $x > 0$) have been highlighted as potential materials for solar energy applications due to appropriate band gaps of ∼1.2 eV.[1] In addition, $Cu_{2-x}Se$ ($x \geq 0$) NCs have been recently investigated in terms of electronic properties.[3] Impressive efforts have been made to develop synthesis strategies[3−8] leading to copper chalcogenide NCs of controlled sizes,[4,9−11] shapes,[9,12,13] and composition.[3,12−15] Due to their nanometer size range, NCs possess unique size-dependent optical properties that are not present in bulk solids.[16] Confinement of charge carriers within a restricted volume leads to a continuous shift of the excitonic transitions in semiconductor NCs. This results in tunable optical properties, providing an excellent tool for nanoscale design of, for example, photovoltaic devices. On the other hand, metal nanoparticles, with their high density of charge carriers, have been the focus of attention in recent years. Their optical properties, dominated by localized surface plasmons (LSPs), are size and shape dependent[17] and show potential for use in bioimaging[18] and photothermal therapy.[19] One particularly interesting class of colloidal nanostructures are hybrid nanoparticles that combine different material properties, such as semiconducting and metallic, in one nanosystem.[20] The interest in such structures is driven by electronic interactions in the excited state such as energy transfer,[21] local field enhancement,[22] photocatalysis,[23] or exciton plasmon interactions.[21] Up to now these hybrid heterostructures were mainly based on self-assembly,[24] upon linking of the components with DNA molecules or decoration of semiconductor nanostructures with metals.[25]

Recently, research in the field of semiconductor NCs has focused toward a new class of material in which the effect of self-doping leads to the evolution of an LSP in the NIR, for example in $Cu_{2-x}S$ nanoparticles. Luther et al. showed that the

Received: August 17, 2011
Published: December 13, 2011

   dx.doi.org/10.1021/ja207798q | J. Am. Chem.Soc. 2012, 134, 1583−1590

self-doping effect in various types of semiconducting nanocrystals leads to LSPs spanning from the terahertz up to the NIR regime.[26] In particular, copper sulfide in its stoichiometric (Cu_2S) form does not support plasmon resonances, while its nonstoichiometric ($Cu_{2-x}S$) composition develops an LSP extinction band in the NIR. Dorfs et al. demonstrated that exposure of $Cu_{2-x}Se$ NCs either to oxygen or to a Ce(IV) complex results in the development of the NIR plasmon band due to the creation of copper vacancies in the material.[27] This is in agreement with the findings from Luther et al.[26] Further, Dorfs et al. showed that the addition of an excess of Cu^+ ions leads to the reduction of the LSP band in the NIR. The correlation of crystal structure to the plasmonic feature found that no significant changes in the crystal structure occurred during the process of NC oxidation as well as reduction.

In this article, we compare the entire family of copper chalcogenide NCs, namely, $Cu_{2-x}S$, $Cu_{2-x}Se$, and $Cu_{2-x}Te$ ($x \geq 0$), which combine excitonic features and LSPs in one material. We show how the LSP resonance of the NCs can be controlled by different chemical means and study the corresponding photophysics and structural changes. Furthermore, we also show, to the best of our knowledge for the first time, how the evolution of LSPs in this type of NC affects the excitonic transitions. The synthesis of $Cu_{2-x}Te$ NCs, exhibiting similar properties in the NIR as its sulfur and selenium counterparts, is reported here for the first time. Moreover, we show that reduction of the material leads to the total recovery of the initial crystal structure and correlate the tunability of the LSP to the exciton recombination in $Cu_{2-x}S$ NCs. We investigate photoluminescence (PL) quenching and recovery during oxidation and reduction, indicating a complete recovery of the initial optical properties after the full reaction cycle. The plasmonic properties in all three copper chalcogenide materials are investigated by time-resolved absorption spectroscopy showing the typical optical nonlinearities of plasmonic resonances.

2. EXPERIMENTAL SECTION

Synthesis of Cu_2S, Cu_2Se, and $Cu_{2-x}Te$ ($x > 0$) NCs. The synthesis of 5 nm Cu_2S NCs was performed according to a previous report.[2]

In a typical synthesis of $Cu_{2-x}Se$ NCs, 1.2 mmol of Se powder (94.8 mg) was mixed with 9 mL of 1-octadecene (ODE) and 6 mL of Oleylamine (OAm) in a three-neck flask. The mixture was heated to 120 °C and kept for 30 min under vacuum before subsequently heating to 310 °C under nitrogen. The solution turned orange at 310 °C, while a trace amount of Se powder remained undissolved. In another three-neck flask, a mixture of 2.0 mmol of copper(I) chloride (CuCl) (99 mg), 3 mL of ODE, and 2 mL of OAm was heated to 120 °C and kept for 30 min under vacuum to prepare the copper precursor. Thereafter, it was maintained at 120 °C under nitrogen until the solution turned clear. Injection of the copper precursor into the flask containing the Se−ODE−OAm mixture led to an immediate color change to black and to a temperature drop to ca. 285 °C. The temperature was allowed to increase to 300 °C, and the reaction was maintained at the temperature for 20 min before the flask was cooled to room temperature.

To synthesize $Cu_{2-x}Te$ ($x > 0$) NCs, 0.6 mmol of Copper(II) acetylacetonate ($Cu(acac)_2$) (157 mg) was added to a mixture of 6 mL of oleic acid (OA) and 3 mL of 1-dodecanethiol (DDT). The dispersion was subsequently heated to 160 °C to form a clear solution. Once temperature stabilized, 0.2 mL of trioctylphosphine (TOP)-Te (1 M, prepared by dissolving Te shot in TOP) was quickly injected. An immediate color change to black was observed, and the reaction was kept at 160 °C for 30 min.

Separation and Purification of NCs. The reaction mixture was transferred to a glovebox for separation and purification of the Cu_2S, Cu_2Se, and $Cu_{2-x}Te$ ($x > 0$) NCs. First, the crude solution of as-prepared NCs was combined with 8 mL of ethanol and centrifuged for 3 min. The supernatant was discarded, while the precipitate was redispersed in 1.5 mL of hexane/toluene and subsequently flocculated with 3 mL of ethanol followed by centrifugation for 3 min. Finally, the precipitate was redispersed in 6 mL of hexane/toluene, and the NC dispersion was centrifuged for 30 s to remove any poorly capped NCs. The supernatant containing stable NCs was collected and kept in the glovebox for later use.

Structural Characterization. Wide-angle powder X-ray diffraction (XRD) patterns were collected using a Bruker D8 diffractometer with a Cu Kα X-ray source operating at 40 kV and 40 mA and Vantec 2000 area detector. The assignment of crystalline phases was based on the reference files in the Powder Diffraction File (PDF-2) database from International Center for Diffraction Data (ICDD). The XRD patterns of stoichiometric (nonoxidized) Cu_2S/Se NCs were measured after drop-casting (in a glovebox) 10 μL of concentrated NC dispersion in hexane/toluene onto a glass substrate. The substrate was thereafter placed inside a gas-tight sample holder designed for powder XRD analysis of air-sensitive specimens. The XRD pattern of nonstoichiometric (oxidized) $Cu_{2-x}S$ NCs ($x = 0.03$) was measured after exposure of stoichiometric Cu_2S NCs to air for one week. The evolution of the crystalline structure of stoichiometric Cu_2Se NCs upon oxidation was determined by recording the XRD patterns of initially stoichiometric NCs at different times of air exposure over a total period of ca. 5 h. For as-synthesized (nonstoichiometric) $Cu_{2-x}Te$ NCs ($x > 0$), the XRD pattern was measured under ambient conditions.

Optical Characterization. UV−vis−NIR extinction spectra of the NCs were measured in 1 cm path length NIR cuvettes using a Cary 5000 UV−vis−NIR spectrophotometer. For these experiments a dilute dispersion of NCs was prepared inside a glovebox using anhydrous solvents and sealed in a cuvette with screwcap and septum to prevent any oxidation prior to and during the measurement. The evolution of optical properties of the starting, stoichiometric (nonoxidized) Cu_2S/Se NCs in toluene was tracked with time during oxidation in air. For that, the screwcap was removed to allow oxygen diffusion into the colloidal dispersion, followed by gentle sonication. For Cu_2S oxidation, spectra were recorded over a period of 6 days (after 1 h, 7 h, 19 h, 28 h, 48 h, 3 days, 4 days, and 6 days of air exposure). For Cu_2Se oxidation, spectra were measured every 20 min over a period of 10 h.

Reduction Experiments. A colloidal solution of Cu_2Se NCs was drop-casted onto a glass substrate, and the XRD pattern of the sample was measured under a nitrogen atmosphere. The same batch of Cu_2Se NC colloidal solution (100 μL, ~5 mg/mL) was further diluted to the proper concentration. An extinction spectrum was measured before and after exposure to air for 12 h. Subsequently, a portion of 0.02 M toluene solution of diisobutylaluminium hydride (DIBAH) was mixed with the solution of oxidized NCs in a sealed cuvette, and the extinction spectra were recorded every 10 min to monitor changes in the LSP. The addition of DIBAH was repeated several times to fully suppress the plasmonic spectral feature. A total volume of 55 μL of DIBAH was added to 3 mL of the NC dispersion. At the late stage of reduction, a trace amount of OAm was added to preserve the colloidal stability. In a typical XRD experiment, 5 μL of a 1 M solution of DIBAH in toluene was added to a dispersion of $Cu_{2-x}Se$ ($x > 0$) NCs exhibiting a well-defined LSP band at 1290 nm obtained upon oxidation of nearly stoichiometric Cu_2Se NCs ($x \approx 0$) in the presence of oxygen, as discussed above. Finally, ethanol was added to precipitate all reduced Cu_2Se NCs out and to quench excess DIBAH. The XRD pattern of the reduced Cu_2Se NCs was taken in the same air-free way.

PL Experiments. In a typical PL steady state experiment, the $Cu_{2-x}S$ NCs were excited at 450 nm, and a long-pass glass filter (Schott OG590) was used to cut the excitation wavelength. Cu_2S NCs were stored in the glovebox and in anhydrous toluene. For oxidation experiments, extinction and PL spectra were measured in a sealed cuvette before exposing the NCs to air over a period of 10 h. The oxidation process was tracked with time. Extinction and PL spectra were recorded every hour. For reduction experiments, the extinction spectrum of a diluted dispersion of $Cu_{2-x}S$ ($x > 0$) NCs in anhydrous

toluene was recorded in a sealed cuvette and transferred back to the glovebox. Subsequently, 30 μL of a 0.1 M solution of DIBAH was added, and the extinction spectra were recorded over a time period of 5 h. PL spectra were recorded after 4 and 5 h of reaction with DIBAH. For further oxidation experiments, the same cuvette was opened to air for 1 h. Extinction spectra were recorded over a period of 1 h. A PL spectrum was taken after 1 h. The absorption of DIBAH was negligible compared to the optical absorption of NCs. For the fluorescence quantum yield measurements, the absorbance was adjusted to be equal at the excitation wavelength for both sample and reference. The measurement has been corrected for the different solvent refractive indices.

Time-Resolved PL Spectroscopy. Time-resolved PL measurements were performed with a streak camera (Hamamatsu C5680) combined with the spectrometer (Cromex, 40 g/mm grating). The frequency doubled output of a mode-locked titanium-sapphire laser (150 fs, 76 MHz) was used as excitation source at 400 nm.

Transient Absorption. Experiments were performed with a 2 kHz Ti:sapphire amplified laser using the second harmonic at 400 nm for the pump beam and a white light continuum as probe.

Elemental Analysis. For inductively coupled plasma optical emission spectroscopy (ICP-OES) studies, dried $Cu_{2-x}Se$ NCs and $Cu_{2-x}Te$ NCs were dissolved with the half-concentrated aqua regia. The organic surfactants were extracted twice with chloroform. The washed aqueous solution was characterized with ICP-OES. For energy-dispersive X-ray spectroscopy (EDS), concentrated $Cu_{2-x}Te$ colloidal solution was drop-casted onto a silicon wafer and studied using a JEOL 5400LV SEM equipped with EDS.

3. RESULTS AND DISCUSSION

Stoichiometric Cu_2S and Cu_2Se NCs were synthesized via hot-injection methods under air-free conditions (see Experimental Section for details). Representative TEM micrographs of as-prepared NCs are shown in the insets in Figure 1a ($Cu_{2-x}S$, x = 0, ~5 nm) and 1c ($Cu_{2-x}Se$, x = 0, ~12 nm). The respective XRD patterns (black curves in Figure 1b and 1d) indicate that the as-synthesized NCs are nearly stoichiometric, i.e., x = 0. In both cases, the vis-NIR extinction spectra of the NCs (black curves in Figure 1a and 1c) are characterized by a steep rise at short wavelengths, a low intensity onset extending up to ~1000 nm, and negligible NIR extinction.

In contrast to other metal chalcogenide NCs,[28] stoichiometric copper chalcogenides are prone to oxidation into more thermodynamically stable nonstoichiometric copper chalcogenide phases containing both Cu^+ and Cu^{2+} ions. Experiments on bulk samples have shown that the anodic oxidation of Cu_2S films into CuS occurs with a concomitant change in stoichiometry.[29] The extinction spectra displayed in Figure 1a and 1c show that, regardless of the chalcogenide, air exposure leads to the development of an NIR band in the NCs that gradually gains intensity and blue-shifts with increasing oxidation time. Upon oxidation we also observed that the intensity of the lowest interband transition at ca. 800 nm for $Cu_{2-x}S$ and $Cu_{2-x}Se$ decreases, likely affecting excitonic transitions in the NCs. After ca. 10 h under oxidative conditions for Cu_2Se and ca. 6 days for Cu_2S NCs, no further spectral changes were observed. These observations are in good agreement with several recent studies of $Cu_{2-x}S$[26] and $Cu_{2-x}Se$.[27]

The XRD patterns displayed in Figure 1b confirm that the initially stoichiometric 5 nm Cu_2S NCs (black curve) after 6 days of exposure to air transform into the nonstoichiometric $Cu_{2-x}S$ (x = 0.03) phase (red curve), commonly known as djurleite. Figure 1d shows the time evolution of the XRD pattern of the stoichiometric Cu_2Se NCs during air exposure. In

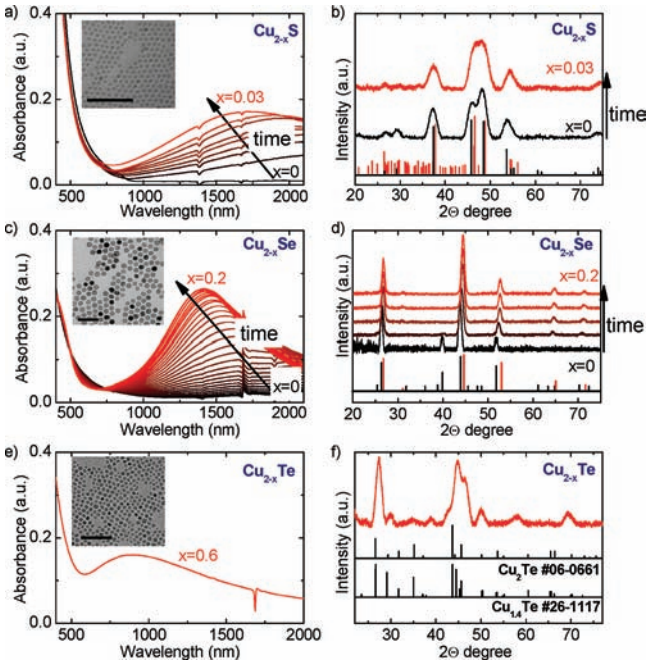

Figure 1. Time evolution of the vis–NIR extinction spectra of stoichiometric (a) $Cu_{2-x}S$ (x = 0, black curve) and (c) $Cu_{2-x}Se$ (x = 0, black curve) NCs in toluene during oxidation upon air exposure for 6 days and 10 h (respectively). With the exposure time, x gradually increases, and at the end of the process (red curves) x = 0.03 for $Cu_{2-x}S$ and x = 0.2 for $Cu_{2-x}Se$, respectively. The insets show the TEM micrograph of the corresponding stoichiometric, nonoxidized, NCs (the scale bar is 50 nm). (b) XRD patterns of the $Cu_{2-x}S$ NCs shown in (a) before (x = 0, black curve) and after (x = 0.03, red curve) 6 days of air exposure. (d) Time evolution of the XRD patterns of the $Cu_{2-x}Se$ NCs shown in (c) during oxidation. From the black to the red curve, the patterns are recorded after 0 (x = 0, black curve), 15, 120, 220, and 320 min (x = 0.2, red curve) of air exposure. In (b) and (d), the vertical bars are the corresponding, color-coded, bulk reference patterns. (e) Vis–NIR extinction spectrum of the as-synthesized $Cu_{2-x}Te$ (x > 0) NCs in toluene. (f) Corresponding XRD pattern of the $Cu_{2-x}Te$ (x > 0) NCs.

the presence of oxygen, stoichiometric tetragonal phase Cu_2Se NCs gradually transform into nonstoichiometric, cubic $Cu_{2-x}Se$ (x = 0.2) NCs, in agreement with previous data.[3] After 15 min of exposure to air, the main peaks at 26.2, 43.8, and 51.8° shift to slightly higher 2θ angles indicating a decrease in the lattice parameters when compared to the original sample. At the same time, two peaks at 38.9 and 39.7°, assigned to the stoichiometric, tetragonal Cu_2Se phase, disappear, while the peaks corresponding to nonstoichiometric, copper-deficient, $Cu_{2-x}Se$ (x > 0) appear at ~65° and 72°. With increasing exposure time (120, 220, 320 min) the pattern further develops into the pattern expected for cubic $Cu_{2-x}Se$ (x = 0.2), suggesting a complete phase transformation of the NCs. In both cases, TEM imaging confirms that the NCs preserve their original shape and size during oxidation (Figure S1 in the Supporting Information), while their stoichiometry and crystal structure evolve during air exposure. Taken together, these data show that there is a clear correlation between the evolution of the NIR band and the transformation from stoichiometric ($Cu_{2-x}S$/Se, x = 0) to nonstoichiometric ($Cu_{2-x}Se$/$Cu_{2-x}S$, x > 0) phases under oxidative conditions. In the NCs, the presence of oxygen drives the oxidation of Cu^+ to Cu^{2+}, thereby creating copper vacancies in the NC core, as recently reported.[3] The

dx.doi.org/10.1021/ja207798q | J. Am. Chem.Soc. 2012, 134, 1583–1590

copper vacancies are responsible for the formation of free carriers (holes) in the nonstoichiometric NCs with mixed Cu^{+}/Cu^{2+} oxidation states.[3,27] As the oxidation proceeds, i.e., as x increases, an increasing number of copper vacancies (free carriers in the NCs' valence band) are created.[27] This gives rise to a higher free carrier absorption in the NIR, which is in agreement with a recently reported ca. 3000-fold higher conductivity of $Cu_{2-x}Se$ (x = 0.2) with respect to Cu_2Se NCs.[3] A high concentration of free carriers in a NC of small dimensions localizes the carriers to a confined space, similar to electrons in metal nanoparticles, leading to LSPs.[14,26] The NIR band blue-shifts and gains intensity during oxidation, i.e., with increasing free carrier concentration, a behavior expected for an LSP.[30] Another typical behavior of the plasmonic feature in nanoparticles is its size dependence as shown in the Supporting Information (Figure S2) for $Cu_{2-x}S$ NCs. With decreasing size of the NCs, the LSP band broadens and red-shifts, whereas for NCs smaller than 3 nm the LSP is completely suppressed. This behavior is in accordance with the findings from Luther et al. and can be attributed to the effect of surface scattering of free carriers.[26,30]

As-synthesized $Cu_{2-x}Te$ NCs show a pronounced LSP band centered around 900 nm (Figure 1e). The inset in Figure 1e displays a representative TEM image of as-prepared, cubic-shaped $Cu_{2-x}Te$ NCs. The XRD pattern shown in Figure 1f cannot unambiguously distinguish between rickardite $Cu_{1.4}Te$ (x = 0.6) and stoichiometric Cu_2Te (x = 0) crystal structures. Figure S3 (Supporting Information) shows powder XRD patterns for four different batches of $Cu_{2-x}Te$ NCs showing batch-to-batch consistency of the crystal structure. We carried out the elemental analysis for as-synthesized $Cu_{2-x}Te$ NC samples. Both ICP−OES (Inductively Coupled Plasma−Optical Emission Spectrometry) of digested NCs and SEM−EDS (Scanning Electron Microscopy−Energy Dispersive Spectroscopy) confirm that the Cu:Te atomic ratio in our NCs was very close to 2:1, suggesting a stoichiometric composition. This observation points to an apparent discrepancy between extinction spectroscopy that reveals an LSP typical for nonstoichiometric NCs (x > 0) and the elemental analysis pointing to x = 0. We will return to this point below. Interestingly, air exposure of as-synthesized copper telluride NCs does not induce changes of the optical extinction spectrum.

All copper chalcogenide NCs exhibit plasmonic properties. Fully air-oxidized $Cu_{2-x}Se$ NCs reach values of x up to 0.2,[27] whereas fully oxidized $Cu_{2-x}S$ NCs reach values of up to 0.03. The higher value of x, i.e., higher number of copper vacancies, in $Cu_{2-x}Se$ NCs with respect to $Cu_{2-x}S$ is related to a more blue-shifted LSP and with this to a higher charge carrier density.[26,27] The charge carrier density extracted from the plasmon frequency[26,27] for those two types of copper chalcogenide NCs gives values of 1.4 × 10^{21} cm^{-3} and 3 × 10^{21} cm^{-3}, respectively, showing the expected trend of increasing charge carrier density with increasing x. The calculated value for the charge carrier density from the plasmon frequency in $Cu_{2-x}Te$ NCs is 5 × 10^{21} cm^{-3}. This suggests a higher value of x with respect to the other copper chalcogenide compounds which is, again, in apparent contradiction with the elemental analysis showing nearly stoichiometric Cu_2Te composition.

Additional tunability of the NIR LSP can be achieved by the addition of a strong reducing agent, diisobutylaluminium hydride (DIBAH), to a dispersion of nonstoichiometric copper chalcogenide NCs (Figure 2). As shown in Figure 2a, in the presence of DIBAH, the LSP of the oxidized $Cu_{2-x}Se$ NCs (x > 0, black curve in Figure 2a) significantly red-shifts and decreases in intensity until it nearly vanishes ($x \approx 0$, red curve). The spectra displayed in Figure 2a also indicate that the reaction with DIBAH results in a red shift and intensity increase in the region of the interband transition at ca. 800 nm. XRD analysis confirms that before reduction (black pattern, Figure 2b and c) the crystal structure of the NCs is ascribed to nonstoichiometric, cubic $Cu_{2-x}Se$ (x = 0.2). After reduction with DIBAH (red pattern, Figure 2b and c), the NCs recover their original, stoichiometric (Cu_2Se, $x \approx 0$), tetragonal crystal structure (blue pattern, Figure 2b and c). Our results suggest that the electrons injected by the strong reducing agent to the NCs may drive the reduction of Cu^{2+} to Cu^{+}, entailing a decrease in the number of copper vacancies, i.e., a reduced number of free charge carriers, and hence a gradual red-shift and decrease in intensity of the NIR LSP band. In contrast to the recent work by Dorfs et al.,[27] in which additional Cu^{+} ions were used to transform $Cu_{2-x}Se$ into Cu_2Se NCs, under our reductive conditions the crystal structure of our NCs changes along with their stoichiometry, from nonstoichiometric (x > 0) to stoichiometric ($x \approx 0$). Our data unambigously show that it is possible to reversibly tune the stoichiometry of copper chalcogenide NCs upon oxidation and reduction. We were able to suppress the plasmonic band in $Cu_{2-x}Te$ NCs by adding DIBAH, as well through the introduction of a mild reducing agent tetrakis(acetonitrile)copper(I) hexafluorophosphate ($[Cu(CH_3CN)_4][PF_6]$) used in ref 27 (Supporting Information Figure S4a). Subsequent exposure of the reduced NCs to air restores the LSP band to approximately its original extent (Supporting Information Figure S4b). Additional tunability of the NIR LSP is achieved by changing the dielectric environment of the NCs, by changing the degree of close-packing,[31] or

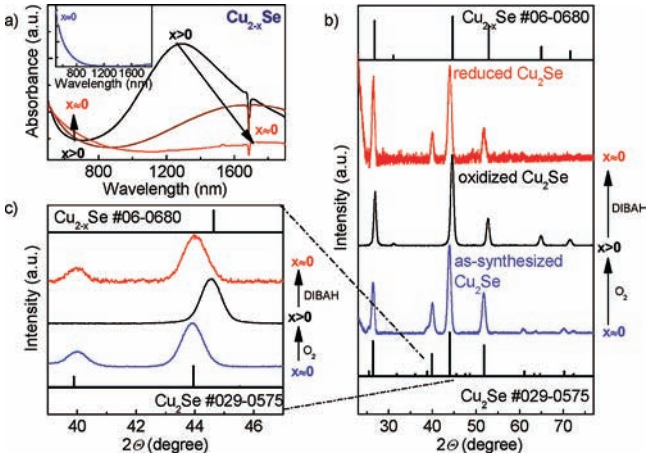

Figure 2. (a) Evolution of the NIR extinction spectra upon the addition of diisobutylaluminium hydride (DIBAH) to $Cu_{2-x}Se$ (x > 0) NCs (elapsing exposure time from black to red curve). Inset: Extinction spectrum of nonoxidized sample. (b) Diffraction patterns for nonoxidized, as-synthesized Cu_2Se NCs (blue curve), oxidized $Cu_{2-x}Se$ (x > 0) (black curve), and reduced Cu_2Se NCs (red curve) together with the respective reference patterns. (c) Enlarged region of the diffraction patterns in (b) illustrating the most significant shifts of diffraction peaks during the solid state conversion from nonoxidized Cu_2Se NCs (blue curve) to oxidized $Cu_{2-x}Se$ (x > 0) (black curve) and reduced Cu_2Se NCs (red curve).

dx.doi.org/10.1021/ja207798q | J. Am. Chem.Soc. 2012, 134, 1583−1590

by switching from OAm to AsS_3^{3-} surface ligands[32] (Figures S5–S7 in the Supporting Information).

The experiments shown above raise the question about the mechanism of copper removal and insertion from/into the lattice upon NC oxidation and reduction, respectively. Does Cu(II) leave the NCs in the form of molecular species that diffuse into the bulk of solution? To test this hypothesis we gently precipitated nonoxidized and oxidized copper selenide NCs and inspected both supernatants by ICP–OES. We found that copper concentrations in both supernatants were very low (3.4 and 1.9 mg/L, respectively). If removed copper entered the solution in the form of molecular species, we expected a significant increase of copper concentration in the supernatant of oxidized $Cu_{2-x}Se$ NCs. If 10% of copper present in our Cu_2Se NCs diffused into solution, the concentration of Cu(II) in supernatant had to rise to 50 mg/L, which was not observed. Therefore, we suggest that Cu species form a thin layer at the NC surface (presumably in the form of CuO or as a monolayer of Cu(II) atoms bound to surface ligands). In fact, a similar mechanism was observed during the oxidation of Cu_2Se NC films in the absence of solvent.[3] Moreover, our experiments on reducing $Cu_{2-x}Se$ NCs with DIBAH (instead of previously used $[Cu(CH_3CN)_4][PF_6]$ reducing agent[27]) clearly indicate that Cu ions can be reinserted into the lattices from these surface layers rather than from an external copper source. Further, as stated above, the determined Cu:Te ratio of 2:1 in our $Cu_{2-x}Te$ NCs with a pronounced LSP feature in the absorption spectrum can be explained by the fact that Cu(II) species remain bound to the NC surface and contribute to the overall Cu:Te ratio. Our results suggest that Cu(II) does not leave copper chalcogenide NCs during the oxidation/reduction cycle.

The evolution of the NIR LSP band seems to have a significant effect on the interband transition of copper chalcogenide NCs in both the oxidation (Figure 1a and b) and reduction experiments (Figure 2a). In the following, we will focus on the effect of the LSP on the excitonic transitions of copper sulfide NCs (~5 nm). In Cu_2S NCs the interband transition is characterized by broad excitonic features, with the blue-shift of the absorption onset with decreasing NC size (Figure S8 in the Supporting Information). Cu_2S NCs show a very low fluorescence quantum yield Φ_f of 4.7×10^{-4}. This value has been determined relative to a standard reference IR140 (Figure S9 in the Supporting Information). This very low fluorescence quantum yield may be due to the band structure that is characterized by an indirect lowest-energy transition and surface traps as discussed below. Nevertheless, PL spectroscopy is a powerful tool to investigate radiative recombination associated with such excitonic transitions in NCs. The black curve in Figure 3a corresponds to the PL spectrum of Cu_2S NCs before exposure to air. The same sample was then exposed to air for a few seconds to allow oxygen diffusion into the previously sealed cuvette, and spectra were recorded after 1, 2, 4, and 10 h. While the NIR LSP is gradually evolving with time of oxygen exposure (Figure 3a, inset), a quenching of PL intensity by a factor of ~2 is obvious after the first hour of oxidation (Figure 3a, black to red curves). The inset to Figure 3a correlates the evolution of the LSP (i.e., the increase in charge carrier density) and the quenching of the excitonic recombination as a function of air exposure time. Next, we triggered the reduction of slightly oxidized $Cu_{2-x}S$ ($x > 0$) NCs by the addition of DIBAH. The black curve in Figure 3b corresponds to a slightly oxidized $Cu_{2-x}S$ ($x > 0$) NC sample. It shows weak PL intensity and exhibits an LSP in the NIR (black curve, Figure 3b, inset). Upon reaction with DIBAH, the LSP gradually red-shifts and decreases in intensity until the spectrum resembles that of nonoxidized Cu_2S NCs ($x \approx 0$) (Figure 3b inset, red curve). At the same time, the PL spectra (Figure 3b, black to red curve) show a significant recovery of PL intensity. Our results suggest that a recovery of the initial interband transitions takes place. This is related to the Burstein–Moss effect of heavily doped semiconductors, which involves a blue-shift of the absorption edge for the oxidized (nonstoichiometric) NCs.[33] After complete reaction with DIBAH, the measured PL intensity exceeds the intensity of the initial, nonoxidized sample (blue curve in Figure 3b). This indicates that the Cu_2S NCs, although not exhibiting a detectable NIR LSP before oxygen exposure, are slightly oxidized, thus already carrying a significant number of free charge carriers contributing to PL quenching.

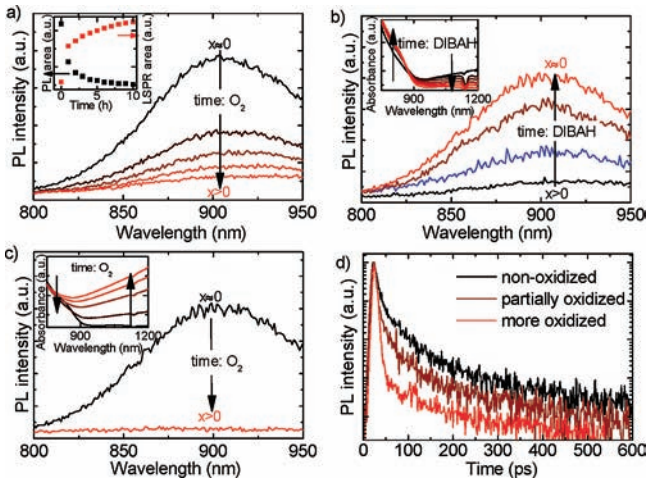

Figure 3. Time evolution of the PL spectra of $Cu_{2-x}S$ NCs in toluene during oxidation upon air exposure (a), subsequent reduction upon the addition of a reducing agent (DIBAH) (b) and re-oxidation upon air re-exposure (c). (a) With exposure time to oxygen, PL intensity is quenched (black to red curves). Inset: integrated PL intensity and extinction at the LSP band as a function of oxidation time. (b) PL intensity increases with time upon the addition of DIBAH (black to red curve) until it exceeds the intensity of the sample before being exposed to air (blue curve). Inset: evolution of the NIR extinction of the same NCs upon the addition of DIBAH. The arrows indicate the observed changes at the NIR LSP band and absorption band onset. (c) By re-exposing the previously DIBAH-reduced NCs to oxygen, the PL intensity is quenched. Inset: evolution of the NIR extinction spectra of the same NCs upon re-exposure to air. (d) Time-resolved PL spectra of nonoxidized and oxidized $Cu_{2-x}S$ ($x \geq 0$) NCs. In all cases, the NCs were excited with a 400 nm laser pulse. The extent of oxidation increases from the black curve (nonoxidized, $Cu_{2-x}S$, $x_1 = 0$) to the brown (partially oxidized, $Cu_{2-x_2}S$, $x_2 > 0$) and red curve (more oxidized, $Cu_{2-x_3}S$, $x_3 > x_2$).

In a subsequent experiment (Figure 3c), the process of oxidation was repeated with the previous sample by opening the cuvette to air for a few seconds. Initially the sample does not exhibit absorption in the NIR (black curve, Figure 3c, inset), which evolves after exposure to air, giving rise again to a complete PL quenching, in agreement with the results presented in Figure 3a. We also observed that the oxidation kinetics (in terms of the evolution of the NIR LSP band) of stoichiometric Cu_2S NCs obtained upon reduction with DIBAH is much faster than that of as-synthesized NCs (Figure 3a). This suggests that the reduced sample is in a more labile

dx.doi.org/10.1021/ja207798q | J. Am. Chem.Soc. 2012, 134, 1583–1590

state. To summarize, a reversible effect on the excitonic transitions can be achieved in our NCs: either a PL quenching upon oxidation or a PL recovery upon reduction. When exposed to air the charge carrier density in our NCs is increased (LSP evolution). This leads to a higher probability of nonradiative recombination. The addition of a reducing agent decreases the density of free holes, inducing a recovery of PL intensity.

The effect of LSPs on the excitonic transitions has been investigated by means of time-resolved PL spectroscopy (Figure 3d). While the plasmon band in the NIR is increasing, the PL intensity is quenched with a shortening of the exciton lifetime. All three decays are well described by a biexponential fit, showing a fast initial component of 10 ps, corresponding to the time resolution of our setup, and a second decay on a longer time scale (100 ps). The increasing amplitude of the fast component with oxidation is reminiscent of a multiparticle interaction already observed in II–VI NCs, such as Auger recombination.[34] Such a process is expected since free holes can interact with the electron hole pair constituting the exciton. However, we do not exclude that carrier trapping may lead to a substantial quenching of PL. Trapping sites might be related to the increase in copper vacancies in the oxidized NCs. Another mechanism for PL quenching is the energy transfer from the exciton to the plasmon, a process which has been well characterized for chromophores in proximity of metal nanoparticles. As discussed for the data in Figure 3b, as-synthesized Cu_2S NCs might have a significant number of free carriers responsible for the fast decay in this sample.

To characterize the LSP dynamics and compare it to the one of excitons, we performed transient absorption studies on $Cu_{2-x}S$ ($x > 0$), $Cu_{2-x}Se$ ($x > 0$) NCs, and $Cu_{2-x}Te$ ($x > 0$) NCs. The pump fluence was 1620, 1410, and 570 $\mu J/cm^2$, respectively. Similar results were obtained over the investigated pump fluence range with a linear dependence of the amplitude of the transient signal on the incident pump power (Figure S10 in the Supporting Information). Figure 4a and c shows that after excitation with a 100 fs laser pulse in resonance with the interband absorption region (400 nm) an optical nonlinearity is observed in the spectral range of the LSP for $Cu_{2-x}S$ ($x > 0$) and $Cu_{2-x}Se$ ($x > 0$) NCs, respectively (Figure 4 a and c). The observed feature in the differential spectrum suggests both a red shift and a broadening of the LSP band with respect to the steady state absorption. The temporal evolution of the LSP photoinduced signal at 1250 nm for $Cu_{2-x}S$ ($x > 0$) and 1200 nm for $Cu_{2-x}Se$ ($x > 0$) NCs is shown in Figure 4b and d and is described by a two-step decay. The first part takes place within the first 3 ps with a time constant smaller than 1 ps. The second, longer exponential decay occurs on a time scale longer than 500 and 1000 ps, respectively, with time constants of approximately 85 and 250 ps. The inset to Figure 4b and d shows the time evolution of the transient signal on a shorter time scale, which highlights an initial rise. The spectra of the nonlinearity observed for $Cu_{2-x}Te$ NCs are displayed in Figure 4e. The spectrum spans a spectral range where the white light used as a probe beam has a peak (~800 nm). This explains the gap in the data constituting these spectra. Nevertheless, in Figure 4f we report the temporal evolution of the LSP photoinduced signal at 730 nm for $Cu_{2-x}Te$ ($x > 0$) NCs. The two-step decay as observed for $Cu_{2-x}S/Se$ ($x > 0$) NCs with a fast component decaying within the first picoseconds and a second longer decay is also apparent (time constants are 1.5 and 300 ps, respectively).

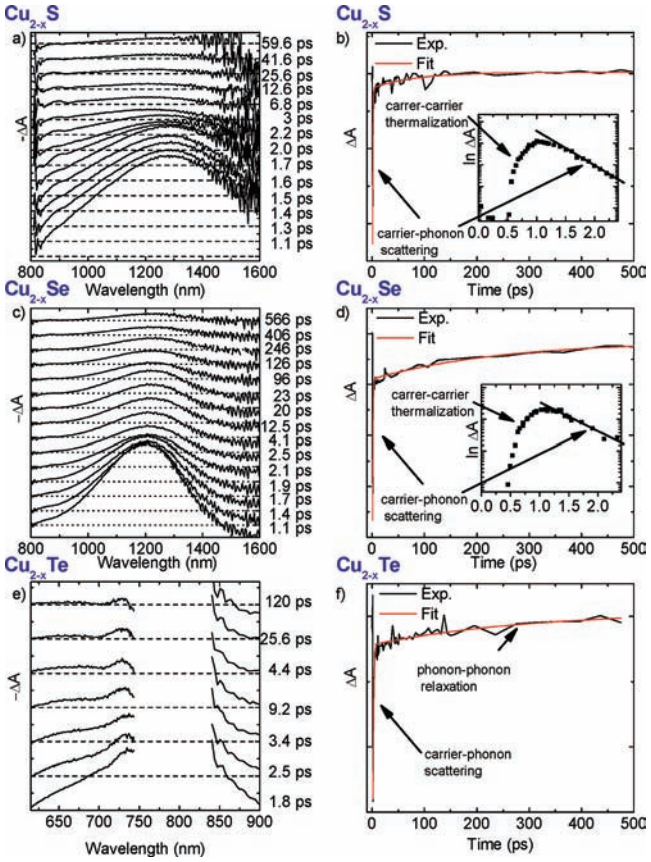

Figure 4. (a), (c), and (e) Transient absorption spectra of $Cu_{2-x}S/Se/Te$ ($x > 0$) NCs after excitation at 400 nm with a 100 fs pulsed laser at different time delays. (b) and (d) Recovery of the transient absorption signal monitored at the bleach maximum (1250 and 1200 nm, respectively) together with a biexponential fit. Inset: Electron–electron thermalization. (Note that this kinetic trace was originally a transient bleach signal before applying the natural logarithm.) (f) Recovery of the transient absorption signal of $Cu_{2-x}Te$ NCs monitored at 730 nm with a biexponential fit.

In noble metals, transient absorption can be used to study the carrier dynamics and the interaction between carriers and between carriers and lattice vibrations (phonons). The differential spectra show a nonlinearity in the region of the surface plasmon resonance caused by an optically induced red-shift and broadening of the LSP. A broadening of the LSP reflects the pump- induced damping of the LSP resonance, which is due to scattering between the charge carriers and with phonons, and lattice defects or disorders.[35,36] The initial red-shift of the LSP is caused by the change of the dielectric properties triggered by the laser-induced heating of the carrier gas. The pump pulse induces transitions far above the Fermi level which create a nonthermal distribution of charge carriers. After equilibration of the charge carriers via carrier–carrier scattering, this distribution can be described by a Fermi distribution function with an associated higher carrier temperature.[35,37] The time taken by the LSP peak to reach its largest red-shift is considered to be the carrier–carrier thermalization time.[36] The following decay of the nonlinearity is described by a two-step process. The hot carriers cool down via the emission of optical phonons, thereby heating the lattice rapidly.[38] This is also the time the red-shift takes to blue-shift back to its initial value. The temperature equilibration between the carriers and the lattice leaves the system at a higher temperature. This is

dx.doi.org/10.1021/ja207798q | J. Am. Chem.Soc. 2012, 134, 1583–1590

reflected in the remaining long decaying nonlinearity, which is attributed to a heat transfer from the particle to the surrounding medium.[35] In metals, carrier−carrier thermalization is expected to occur on the times comparable to the duration of the laser pulse because of the high electron density. It manifests itself as a slower rise time of the transient signal[39] on the time scale of 500 fs.[38] The equilibration between electrons and the lattice (carrier-phonon scattering) is expected to be longer and can, thus, be followed in real time with femtosecond spectroscopy.[37] In noble metals, the electron−phonon scattering was found to be on the order of a few picoseconds (1−4 ps), whereas the time constant of the second, longer, decay has been measured to be around ∼100 ps.[39]

The nonlinearities in the dynamics of plasmonic features can be explained by changes in the dielectric function of the investigated metallic structure. These are induced by elevated carrier and lattice temperatures (T_C and T_L), as explained above, and identified as two-step decays in the kinetics of the differential spectra. To investigate the time evolution of the carrier and lattice temperatures, the two-temperature model (TTM) has been introduced for metal nanoparticles.[40] The precise quantitative value of the differential absorption depends on details of the dielectric function, and its calculation exceeds the scope of this work. Nevertheless, in a work from Scotognella and co-workers published recently, the TTM has successfully been applied to $Cu_{2-x}Se$ NCs.[41] The time dependence of the temperatures T_C and T_L has been identified and thoroughly discussed.

Our results suggest that the carriers in our copper chalcogenide NCs behave similar to those in noble metal nanoparticles. A pump-induced nonlinearity is observed in the transient spectra. A broadening of the LSP is observed that reflects itself in a positive component on the blue and red side of the differential spectrum. The positive component on the red side of the differential spectrum is identified for $Cu_{2-x}Se$ NCs. For $Cu_{2-x}S$ NCs, this part is too far in the red and cannot be resolved with our measurement setup. On the blue side of the spectrum, the positive component is not apparent in both spectra. This may be due to an overlaying component from the bleaching of the indirect transition which is dominant in this wavelength regime. A red-shift of the LSP maximum is observed, in the differential spectra, which builds up within ∼1 ps, along with a shift back to a constant value within the first 4 ps (Figure S11 in the Supporting Information), in agreement with the thermalization and cooling of the carrier gas.

However, this rise might be as well due to energy transfer from the exciton to the plasmon. The limited time resolution of our time-resolved PL experiments does not allow us to obtain reliable data on the first part of the decay, likely ≪ 10 ps, which might be related to the decay of a hot exciton into the plasmonic excitation via energy transfer. We also observe that our particles have increasing decay times for the second decay ascribed to phonon−phonon relaxation when going from $Cu_{2-x}S$ to $Cu_{2-x}Se$ and $Cu_{2-x}Te$ NCs. At the same time, the ionicity of the chemical bonds inside the nanocrystals is changing when going from one material to the other. This long decay time for the phonon−phonon scattering is another difference with respect to metallic nanoparticles. This difference can be explained considering that chemical bonding in the lattice of copper chalcogenides has a strong ionic component and therefore different acoustic phonons. This leads to a lower heat conductivity compared to noble metals.

4. CONCLUSIONS

In this work, we have discussed the tunability and control over the optical properties (extinction and photoluminescence) of copper chalcogenide NCs ($Cu_{2-x}S$, $Cu_{2-x}Se$, and $Cu_{2-x}Te$, $x \geq 0$) through the active manipulation over their copper deficiency under oxidative/reductive conditions. The presence of NIR LSP resonances in this type of NCs has a significant effect on the exciton recombination. As shown for Cu_2S NCs, their PL is quenched during their gradual transformation into non-stoichiometric NCs ($x > 0$) under oxidative conditions, i.e., as the NIR plasmon band evolves. This PL quenching may result from an Auger-type recombination due to the high charge carrier density in the NCs. Importantly, we have shown that the process can be fully reversed through subsequent transformation of nonstoichiometric $Cu_{2-x}S$ NCs ($x > 0$) into stoichiometric ones ($x \approx 0$) under reductive conditions, i.e., during the gradual disappearance of their NIR LSP band. Finally, we have demonstrated through transient absorption measurements that the NIR LSP resonance in nonstoichiometric $Cu_{2-x}S/Se/Te$ ($x > 0$) NCs behaves analogously to LSP resonances in noble metal nanoparticles. As shown herein, copper chalcogenide NCs offer the unique possibility of holding highly tunable LSP resonances and excitons on demand, and hence they are envisaged as appealing nanoscale elements overcoming the current limitations of hybrid metallic/semiconductor nanostructures. For instance, an improvement over the PL quantum yield of stoichiometric copper chalcogenide NCs may enable their utilization as both fluorescent labels (when nonoxidized) and NIR plasmonic absorbers for photothermal therapy (when oxidized). Whereas we foresee a huge potential of this type of NCs in NIR plasmonic applications, our results suggest that their high tendency to oxidation, and hence to LSP evolution, needs to be taken into account in relation to their prospective application in photovoltaics.

■ ASSOCIATED CONTENT

Supporting Information

Details on the effect of the solvent refractive index, ligands, and close-packing on the LSP resonances of $Cu_{2-x}S/Se$ ($x > 0$) NCs and further optical and structural properties. This material is available free of charge via the Internet at http://pubs.acs.org.

■ AUTHOR INFORMATION

Corresponding Author

enrico.dacomo@physik.uni-muenchen.de; dvtalapin@uchicago.edu

Author Contributions

⊥These authors contributed equally to this work.

■ ACKNOWLEDGMENTS

The Nanosystems Initiative Munich (NIM) and the LMUexcellent program of the DFG are kindly acknowledged. We also thank the BMBF through the project OPV-stability and the EU commission through the ICARUS Marie Curie Research Training Network for financial support. The work was partially supported by NSF CAREER under Award Number DMR-0847535 and by the David and Lucile Packard Foundation. Analytical Chemistry Laboratory at Argonne National Lab (ANL) provided ICP−OES elemental analysis.

REFERENCES

(1) Wadia, C.; Alivisatos, A. P.; Kammen, D. M. *Environ. Sci. Technol.* **2009**, *43*, 2072−2077.
(2) Wu, Y.; Wadia, C.; Ma, W.; Sadtler, B.; Alivisatos, A. P. *Nano Lett.* **2008**, *8*, 2551−2555.
(3) Riha, S. C.; Johnson, D. C.; Prieto, A. L. *J. Am. Chem. Soc.* **2011**, *133*, 1383−1390.
(4) Han, W.; Yi, L.; Zhao, N.; Tang, A.; Gao, M.; Tang, Z. *J. Am. Chem. Soc.* **2008**, *130*, 13152−13161.
(5) Li, S.; Wang, H.; Xu, W.; Si, H.; Tao, X.; Lou, S.; Du, Z.; Li, L. S. *J. Colloid Interface Sci.* **2009**, *330*, 483−487.
(6) Choi, S.-H.; An, K.; Kim, E.-G.; Yu, J. H.; Kim, J. H.; Hyeon, T. *Adv. Funct. Mater.* **2009**, *19*, 1645−1649.
(7) Zhang, H.; Zhang, Y.; Yu, J.; Yang, D. *J. Phys. Chem. C* **2008**, *112*, 13390−13394.
(8) Deka, S.; Genovese, A.; Zhang, Y.; Miszta, K.; Bertoni, G.; Krahne, R.; Giannini, C.; Manna, L. *J. Am. Chem. Soc.* **2010**, *132*, 8912−8914.
(9) Saunders, A. E.; Ghezelbash, A.; Smilgies, D.-M.; Sigman, M. B.; Korgel, B. A. *Nano Lett.* **2006**, *6*, 2959−2963.
(10) Larsen, T. H.; Sigman, M.; Ghezelbash, A.; Doty, R. C.; Korgel, B. A. *J. Am. Chem. Soc.* **2003**, *125*, 5638−5639.
(11) Zhuang, Z.; Peng, Q.; Zhang, B.; Li, Y. *J. Am. Chem. Soc.* **2008**, *130*, 10482−10483.
(12) Lim, W. P.; Wong, C. T.; Ang, S. L.; Low, H. Y.; Chin, W. S. *Chem. Mater.* **2006**, *18*, 6170−6177.
(13) Sigman, M. B.; Ghezelbash, A.; Hanrath, T.; Saunders, A. E.; Lee, F.; Korgel, B. A. *J. Am. Chem. Soc.* **2003**, *125*, 16050−16057.
(14) Zhao, Y.; Pan, H.; Lou, Y.; Qiu, X.; Zhu, J.; Burda, C. *J. Am. Chem. Soc.* **2009**, *131*, 4253−4261.
(15) Ghezelbash, A.; Korgel, B. A. *Langmuir* **2005**, *21*, 9451−9456.
(16) Murray, C. B.; Kagan, C. R.; Bawendi, M. G. *Annu. Rev. Mater. Sci.* **2000**, *30*, 545−610.
(17) Kelly, K. L.; Coronado, E.; Zhao, L. L.; Schatz, G. C. *J. Phys. Chem. B* **2003**, *107*, 668−677.
(18) Anker, J. N.; Hall, W. P.; Lyandres, O.; Shah, N. C.; Zhao, J.; Van Duyne, R. P. *Nat. Mater.* **2008**, *7*, 442−453.
(19) Huang, X.; El-Sayed, I. H.; Qian, W.; El-Sayed, M. A. *J. Am. Chem. Soc.* **2006**, *128*, 2115−2120.
(20) Mokari, T.; Rothenberg, E.; Popov, I.; Costi, R.; Banin, U. *Science* **2004**, *304*, 1787−1790.
(21) Zhang, W.; Govorov, A. O.; Bryant, G. W. *Phys. Rev. Lett.* **2006**, *97*, 146804.
(22) Govorov, A. O.; Bryant, G. W.; Zhang, W.; Skeini, T.; Lee, J.; Kotov, N. A.; Slocik, J. M.; Naik, R. R. *Nano Lett.* **2006**, *6*, 984−994.
(23) Berr, M.; Vaneski, A.; Susha, A. S.; Rodríguez-Fernández, J.; Döblinger, M.; Jäckel, F.; Rogach, A. L.; Feldmann, J. *Appl. Phys. Lett.* **2010**, *97*, 093108−3.
(24) Shevchenko, E. V.; Ringler, M.; Schwemer, A.; Talapin, D. V.; Klar, T. A.; Rogach, A. L.; Feldmann, J.; Alivisatos, A. P. *J. Am. Chem. Soc.* **2008**, *130*, 3274−3275.
(25) Vaneski, A.; Susha, A. S.; Rodríguez-Fernández, J.; Berr, M.; Jäckel, F.; Feldmann, J.; Rogach, A. L. *Adv. Funct. Mater.* **2011**, *21*, 1547−1556.
(26) Luther, J. M.; Jain, P. K.; Ewers, T.; Alivisatos, A. P. *Nat. Mater.* **2011**, *10*, 361−366.
(27) Dorfs, D.; Härtling, T.; Miszta, K.; Bigall, N. C.; Kim, M. R.; Genovese, A.; Falqui, A.; Povia, M.; Manna, L. *J. Am. Chem. Soc.* **2011**, *133*, 11175−11180.
(28) Katari, J. E. B.; Colvin, V. L.; Alivisatos, A. P. *J. Phys. Chem.* **1994**, *98*, 4109−4117.
(29) Koch, D. F. A.; McIntyre, R. J. *J. Electroanal. Chem.* **1976**, *71*, 285−296.
(30) Mulvaney, P. *Langmuir* **1996**, *12*, 788−800.
(31) Kriegel, I.; Rodríguez-Fernández, J.; Como, E. D.; Lutich, A. A.; Szeifert, J. M.; Feldmann, J. *Chem. Mater.* **2011**, *23*, 1830−1834.
(32) Kovalenko, M. V.; Bodnarchuk, M. I.; Talapin, D. V. *J. Am. Chem. Soc.* **2010**, *132*, 15124−15126.
(33) Lukashev, P.; Lambrecht, W. R. L.; Kotani, T.; van Schilfgaarde, M. *Phys. Rev. B* **2007**, *76*, 195202−14.
(34) Schaller, R. D.; Sykora, M.; Jeong, S.; Klimov, V. I. *J. Phys. Chem. B* **2006**, *110*, 25332−25338.
(35) Perner, M.; Bost, P.; Lemmer, U.; von Plessen, G.; Feldmann, J.; Becker, U.; Mennig, M.; Schmitt, M.; Schmidt, H. *Phys. Rev. Lett.* **1997**, *78*, 2192−2195.
(36) Hamanaka, Y.; Hayashi, N.; Nakamura, A.; Omi, S. *J. Lumin.* **1998**, *76*−*77*, 221−225.
(37) Link, S.; El-Sayed, M. A. *Int. Rev. Phys. Chem.* **2000**, *19*, 409−453.
(38) Burda, C.; Chen, X.; Narayanan, R.; El-Sayed, M. A. *Chem. Rev.* **2005**, *105*, 1025−1102.
(39) Link, S.; El-Sayed, M. A. *Annu. Rev. Phys. Chem.* **2003**, *54*, 331−366.
(40) Anisimov, S. I.; Kapeliovich, B. L.; Perel'man, T. L. *Soviet Physics - JETP* **1974**, *39*, 375−377.
(41) Scotognella, F.; Della Valle, G.; Srimath Kandada, A. R.; Dorfs, D.; Zavelani-Rossi, M.; Conforti, M.; Miszta, K.; Comin, A.; Korobchevskaya, K.; Lanzani, G.; Manna, L.; Tassone, F. *Nano Lett.* **2011**, *11*, 4711−4717.